(12) LEVEL III

DNA 4633F

TITANIUM COMBUSTION STUDY

General Electric Company
Re-Entry and Environmental Systems Division
3198 Chestnut Street
Philadelphia, Pennsylvania 19101

8 December 1977

Final Report for Period September 1976—November 1977

CONTRACT No. DNA 001-76-C-0372

APPROVED FOR PUBLIC RELEASE;
DISTRIBUTION UNLIMITED.

THIS WORK SPONSORED BY THE DEFENSE NUCLEAR AGENCY
UNDER RDT&E RMSS CODE B34207T464 N99QAXAA12945 H2590D.

Prepared for
Director
DEFENSE NUCLEAR AGENCY
Washington, D. C. 20305

Destroy this report when it is no longer needed. Do not return to sender.

PLEASE NOTIFY THE DEFENSE NUCLEAR AGENCY, ATTN: TISI, WASHINGTON, D.C. 20305, IF YOUR ADDRESS IS INCORRECT, IF YOU WISH TO BE DELETED FROM THE DISTRIBUTION LIST, OR IF THE ADDRESSEE IS NO LONGER EMPLOYED BY YOUR ORGANIZATION.

UNCLASSIFIED

SECURITY CLASSIFICATION OF THIS PAGE *(When Data Entered)*

REPORT DOCUMENTATION PAGE	READ INSTRUCTIONS BEFORE COMPLETING FORM
1. REPORT NUMBER: DNA 4633F / AD-E300 475	2. GOVT ACCESSION NO. / 3. RECIPIENT'S CATALOG NUMBER: DNA, SBIE
4. TITLE *(and Subtitle)*: TITANIUM COMBUSTION STUDY.	5. TYPE OF REPORT & PERIOD COVERED: Final Report for Period Sep[redacted]976—Nov[redacted]977
	6. PERFORMING ORG. REPORT NUMBER: 78SDR2217
7. AUTHOR(s): R. J. Sullivan	8. CONTRACT OR GRANT NUMBER(s): DNA 001-76-C-0372
9. PERFORMING ORGANIZATION NAME AND ADDRESS: General Electric Company, Re-Entry and Environmental Systems Division, 3198 Chestnut Street Philadelphia, Pennsylvania 19101	10. PROGRAM ELEMENT, PROJECT, TASK AREA & WORK UNIT NUMBERS: Subtask N99QAXAA129-45
11. CONTROLLING OFFICE NAME AND ADDRESS: Director Defense Nuclear Agency Washington, D.C. 20035	12. REPORT DATE: 8 Dec[redacted]977
	13. NUMBER OF PAGES: 34
14. MONITORING AGENCY NAME & ADDRESS *(if different from Controlling Office)*	15. SECURITY CLASS *(of this report)*: UNCLASSIFIED
	15a. DECLASSIFICATION/DOWNGRADING SCHEDULE

16. DISTRIBUTION STATEMENT *(of this Report)*

Approved for public release; distribution unlimited.

17. DISTRIBUTION STATEMENT *(of the abstract entered in Block 20, if different from Report)*

18. SUPPLEMENTARY NOTES

This work sponsored by the Defense Nuclear Agency under RDT&E RMSS Code B34207T464 N99QAXAA12945 H2590D.

19. KEY WORDS *(Continue on reverse side if necessary and identify by block number)*

Titanium
Nuclear Cloud
Oxidation

20. ABSTRACT *(Continue on reverse side if necessary and identify by block number)*

A heated titanium structure flying through a nuclear burst dust cloud may experience aerodynamic heating, kinetic energy heating and oxidation. The rate of heat transfer due to oxidation is examined to determine its contribution relative to other mechanisms of heat transfer, and whether an increase in oxidation heat transfer occurs in the presence of water vapor. The results of the investigation show that heat transfer is dominated by particle kinetic energy conversion and aerodynamic heating to a roughened surface. Oxidation heat transfer is negligible at temperatures of interest to the structure.

DD FORM 1 JAN 73 1473 EDITION OF 1 NOV 65 IS OBSOLETE

UNCLASSIFIED

SECURITY CLASSIFICATION OF THIS PAGE *(When Data Entered)*

79 05 05 035

404 884

PREFACE:

This report documents the work completed by the General Electric Company under DNA Contract No. 001-76-C-0372.

This work was sponsored by the Aerospace Systems Division of the Shock Physics Directorate and was conducted during the period September 7, 1976 through November, 1977. The principal Investigator was R. J. Sullivan and the Technical Monitor was Major D. Anderson.

TABLE OF CONTENTS

		Page
PREFACE		1
LIST OF FIGURES		2
1.0	INTRODUCTION AND SUMMARY	5
2.0	TITANIUM OXIDATION	7
	2.1 Kinetics of Oxidation	7
	2.2 Review of SAI Test Data	13
	2.2.1 AEDC Data	13
	2.2.2 SAI Santa Ana Data	13
	2.2.3 Additional Effects	14
3.0	EVALUATION OF OXIDATION INFLUENCE ON MATERIAL THICKNESS REQUIREMENTS	19
	3.1 Introduction	19
	3.2 Stagnation Point Temperature Response	19
	3.3 Conical Section	23
4.0	CONCLUSIONS	25

LIST OF FIGURES

Figure		Page
2-1	Oxidation of Titanium In Air	10
2-2	Comparison Between K_s and K_m ~ From Stringer[3]	11
2-3	Comparison Between SAI/Santa Ana Data and Zavitsanos Data	15
2-4	Comparison Between SAI and Zavitsanos Rate Data	16
2-5	View of Test Sample 28A, AEDC Test (2/26/72) Showing Ignition and Dust Roughened Surface	17
2-6	Detailed Views of Surface Roughness	18
3-1	Schematic of Typical Vehicle	20
3-2	Velocity Vs Altitude for a Typical Boost - Phase Vehicle	21
3-3	Temperature Vs Altitude for Three Stagnation Point Thicknesses	22
3-4	Temperature Response of Cone Tangency for Three Thicknesses	24

1.0 INTRODUCTION AND SUMMARY

Dust and rain impact on Titanium has been studied from the standpoint of material ignition at the stagnation point and strength reduction along the frustum of a vehicle exiting through the atmosphere.

Normal heat transfer to the solid surface results in an increased material temperature due to aerodynamic heating. The additional heating which occurs due to dust particle impact is not completely understood, but this effect is to increase material surface temperature. Added to the sum of aerodynamic heating and kinetic energy conversion will be the exothermic reaction of titanium and air. In a previous study[1] this contribution was negligible at temperatures of interest to missile materials.

Catalytic effects, however, can influence reaction rates, and the basic concern in the present study is whether liquid water or ice crystal impact on heated titanium will result in a catalytic action which will increase oxidation rates or reduce the conditions necessary for ignition.

We make a distinction between the stagnation point and the conic section for several reasons. The stagnation point, of course, is the point of maximum heat transfer due to aerodynamic heating and due to particle impact energy conversion. The stagnation point will, therefore, locally approach temperatures with a higher probability of ignition than the conic section. Once ignited, the combustion will continue even under reduced oxygen flow to the metal surface resulting in rapid consumption of the oxygen fraction in the boundary layer by the burning. The conic section, on the other hand, is the load bearing section of the design, and an increase in the material temperature through higher oxidation rates results in a requirement for greater thickness of titanium with an increased structure weight.

The test data obtained at SAI and AEDC and model development has been well documented in (2), and are not detailed in this report. We will present titanium data not included in (2) and assess the effect of the data on a simulated mission.

2.0 TITANIUM OXIDATION:

2.1 Kinetics of Oxidation:

A theoretical model of titanium oxidation rate has not yet been formulated. In general the data shows that oxidation rates of titanium may follow linear, parabolic or cubic rate laws depending upon the period of oxidation, the temperature of the specimen and the concentration of available species at the solid gas interface and the oxide/metal interface.

Stringer[3] observed that initial rates of oxidation of titanium are parabolic, with a grey, adherent oxide scale forming on the surface. A series of data show that, in general,an equation of the form

$$(x + a) = k (y + b)^n$$

can be written to provide a reasonable approximation to test data. The constants k, a, n and b can be evaluated if we replace x with w, (weight gain of the sample), and y with t, (time of the sample exposure). Stringer's results from Reference (3) show an exponent, n, of 0.55 which is close to a parabolic rate law and indicates a diffusion controlled process.

Discussions with Rosa[4] on the mechanism of titanium oxidation produced esentially the type of physical model given in (2), however allowing for the possibility that titanium metal diffusion occurs through the oxide scale to further complicate the model development on a theoretical basis. At the present time no data exists on metal to scale diffusion rates so this remains a speculative issue for further study.

Zavitsanos[5] experimentally determined oxidation rates of titanium in air at low pressure levels, and since the data received limited distribution it is included in this section.

Figure 2-1 shows a plot of weight gain, w, in micrograms per square centimeter of surface area versus time in minutes for the oxidation of titanium samples in air at low pressure (200-600 microns) and at one atmosphere. The 200 and 600 micron pressure level is extremely low pressure representative of very high altitudes of flight (200 microns is 2×10^{-1} mm of Hg. or 2×10^{-1} torrs).

From Zavitsanos data we can see a pressure effect between the low pressure data (200-600 microns) and the 1 atmosphere data clearly defined. (The data at 1277 K is 2 sets of data, 1 at 200 microns and 1 at 600 microns.)

If we regress the data of Zavitsanos, using an expression similar to that of Stringer, we can evaluate the constants, k, a, n and b in the same fashion as Stringer. For Zavitsanos data the values of a and b are zero, and the values of k and n are shown in Table 1. The equation is of the form:

$$w = k\, t^{n}$$

and we obtain a near linear value of n for the data at 200 microns and we approach Stringer's value of n at 600 microns and one atmosphere. At 200 microns the exponent suggests linear oxidation.

TABLE 2-1 Regression of Zavitsanos Titanium Oxidation Data

Test Conditions		Exponent	Pre Exponent
Temperature ^{o}C	Pressure Microns	(n)	(k)
1087	600	.689	298
979	(1 Atm)	.694	5161
895	200	.909	20
1004	200	.962	50
1090	200	.885	77.22

The 3 test conditions shown at 200 micron pressure condition were evaluated to find the activation energy of the system. A value of 24,850 was determined, very close to the value given by Stringer,[3] for the scale forming rate constant. The data suggests that a linear relationship is followed at the low pressure conditions, and that the process approaches a parabolic relationship at 600$\mu$and 1 atmosphere. Certain deductions on the rate controlling mechanisms can be drawn, but it is unfortunate that more values of pressure were not used to permit evaluation of this effect. It is also possible that gas phase diffusion is limiting the reaction rate.

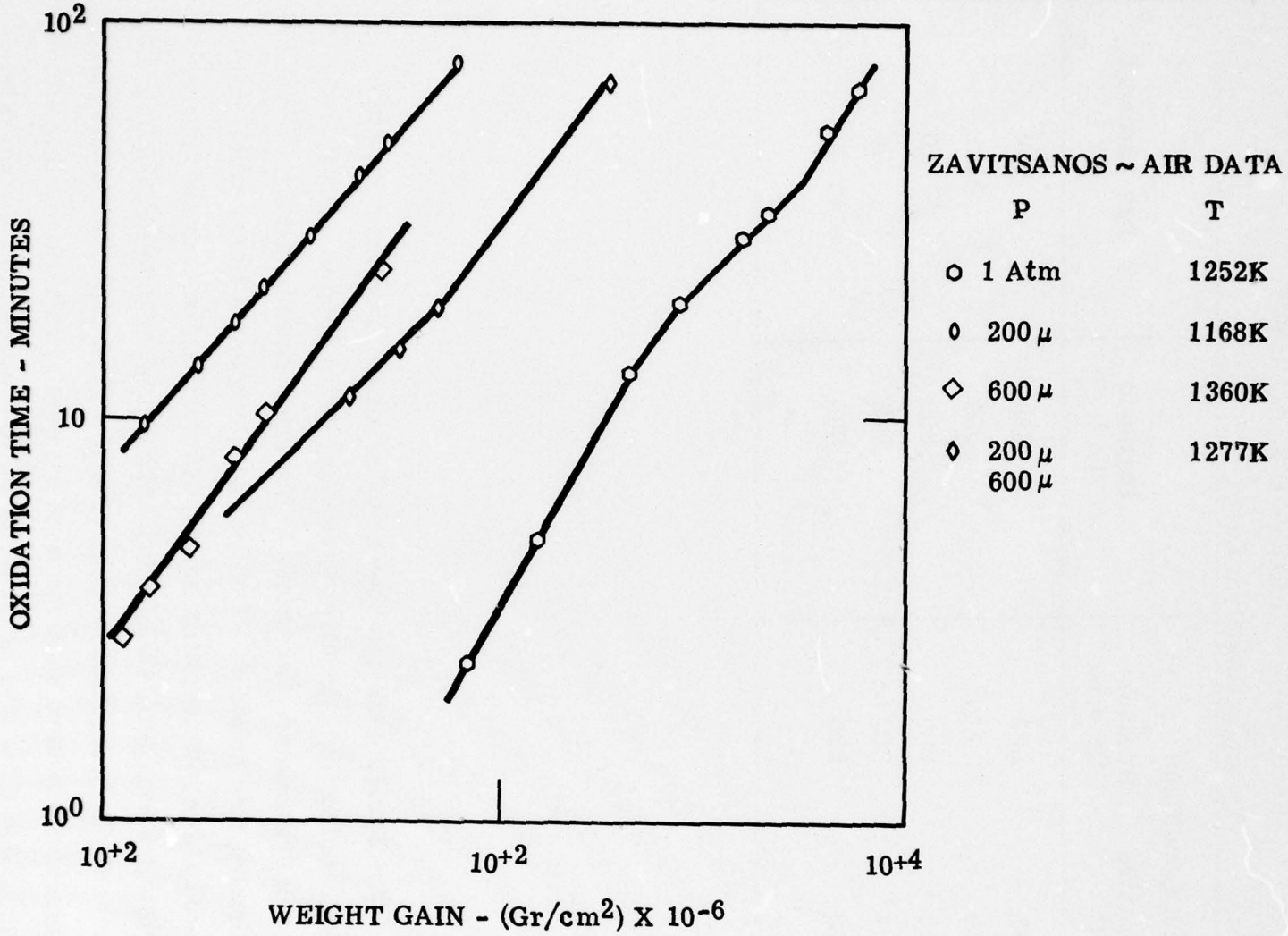

Figure 2-1. Oxidation of Titanium in Air (Ref. 5)

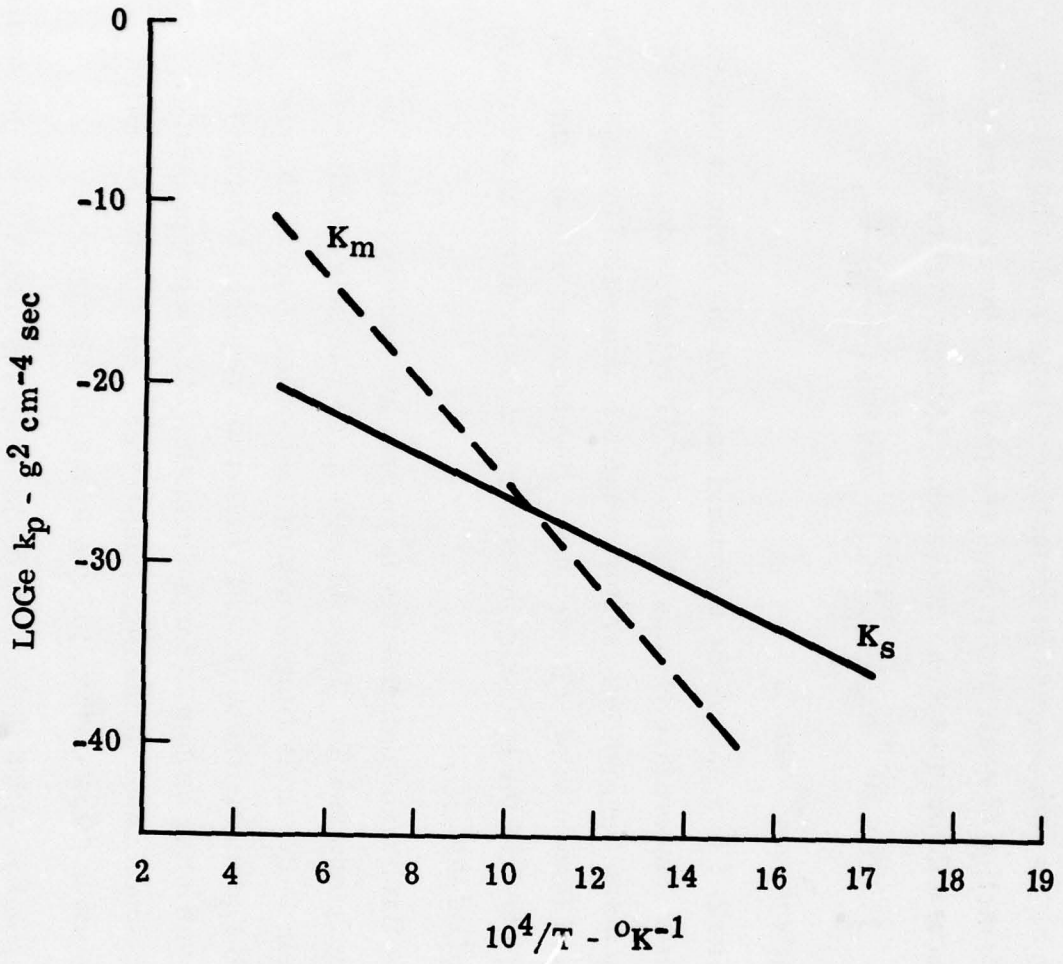

Figure 2-2. Comparison Between K_S and K_M - From Stringer[3]

The controlling factors in Titanium oxidation rates appear to be either scale formation or oxygen dissolution and Stringer has equated these to low temperature and high temperature. The scale forming rate constant, k_s and the dissolution rate constant, k_m, add to form the total rate constant for parabolic oxidation, k_p, with units of $[m^2\ A^{-4}\ t^{-1}]$. The exponential nature of the expression for k_p provides for the majority of weight gain at low temperature in formation of scale and at high temperature in formation of scale and at high temperature the majority of weight gain occurs through oxygen dissolution. Stringer writes this as:

$$k_p = 1.007 \times 10^{-6} \exp\left(\frac{-25400}{RT}\right) + 320 \exp\left(\frac{-61,800}{RT}\right)$$

and k_p has units $g^2\ cm^{-4}\ sec^{-1}$.

Figure 2-2 is a plot of the individual parts of the Stringer equation for k_p. The low temperature regime (large $10^4/T$ value) is dominated by scale formation and the high temperature region is dominated by dissolution. [We tend toward Rosa's view, cited earlier, that titanium diffuses through the oxide scale toward the gas oxide interface and the reaction is a surface reaction based on this.]

Since Zavitsanos data results in an activation energy close to the value Stringer determined for scale formation, we can only conclude that scale formation is the early time dominant controlling item in titanium oxidation, and that an appreciable scale formation requires time at temperature and sufficient oxygen to form the scale. At the low pressure levels of Zavitsanos, even at the high temperature, no significant scale formation occurs to allow control to pass to the dissolution phase.

The point at which the control of the reaction passes from the scale forming rate to the dissolution rate is principally determined by the activation energy, Ea, and only a minor influence of the frequency factor is shown. On Figure 2.2 the increased frequency factor changes the crossing point of the two curves from 10.4 to 10.8 values of $10^4/T$ or 962 K to 925 K. From

this we would now assume that most of the oxidation kinetics on an application would be controlled by the scale forming rate. If the equation of Stringer[3] is applied to shroud oxidation performance the scale forming portion would apply to the sidewall calculation and oxygen solution kinetics would be stronger in the stagnation region. This will be discussed further in Section 3, where we evaluate the shroud heat transfer.

2.2 Review of SAI Test Data:

2.2.1 AEDC Data

A review of the SAI test data obtained on the present program is contained in reference (2) in detail, and the data shows reasonable agreement with literature data.

The AEDC test data conducted on this program showed essentially similar results to the previous dust only studies conducted for Minuteman. The cooling influence of the water adequately described in (2) indicates that the injected water flow broke up under the action of aerodynamic forces and that the erosion effect of the water droplets were minimal. The solid surface of the model quite probably acted to increase the concentration of water vapor locally due to longer residence times of the water molecules in the surface.

The very brief review of the test samples could not confirm that liquid droplets of any significant size had impacted the titanium surface, again indicating that break-up had occurred prior to reaching the model.

2.2.2 SAI/Santa Ana Data

Test data obtained at the SAI/Santa Ana test facility is compared with Zavitsanos data in Figure 2-3, where we show time of oxidation run vs weight gain. As expected the data where only final weight gain is

measured shows a greater degree of inconsistency than continuous readout of a single sample. The initial transient period of oxidation is usually eliminated from continuous data, however for this test we were specifically looking for data in the early time history of oxidation.

The simplest comparison that can be made is based upon rate constant data. We used tha latest published results for several of the oxygen runs quoted in Reference 2, and computed a parabolic rate constant using the weight gain data and the published oxidation times. Again, the assumption of parabolic oxidation is made, and we use:

$$k_p = W^2/t \quad mg^2 cm^{-4} \, min$$

The data agrees well with previously published test results by Kofstad. Figure 2-4 shows the comparison.

2.2.3 Additional Effects

The analysis performed on the kinetics of oxidation was relatively limited. It is felt that the data obtained adequately describes oxidation of titanium in the high temperature regime and provides some evidence that catastrophic ignition will not be iniated earlier in the trajectory due to liquid water or ice impact.

One major item that could prove significant is the larger particle impact during powered flight combined with the surface roughness caused by dust impact. These provide increased surface area for surface absorption, and concave regions for water capture. Figure 2-5 and 2-6 show the roughened surface resulting from small particle dust erosion.

If any further SAI/Santa Ana tests are to be conducted, a roughened surface test should be considered.

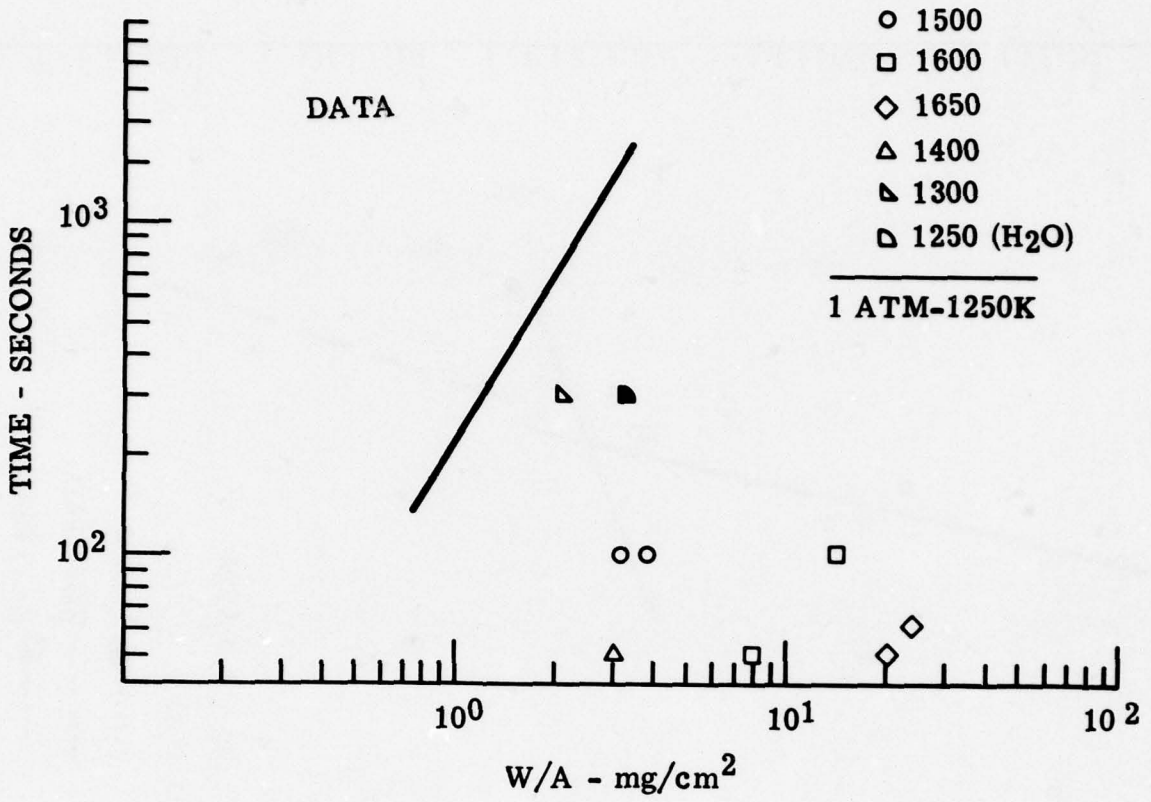

Figure 2-3. Comparison Between SAI (Santa Ana Data and Zavitsanos Data)

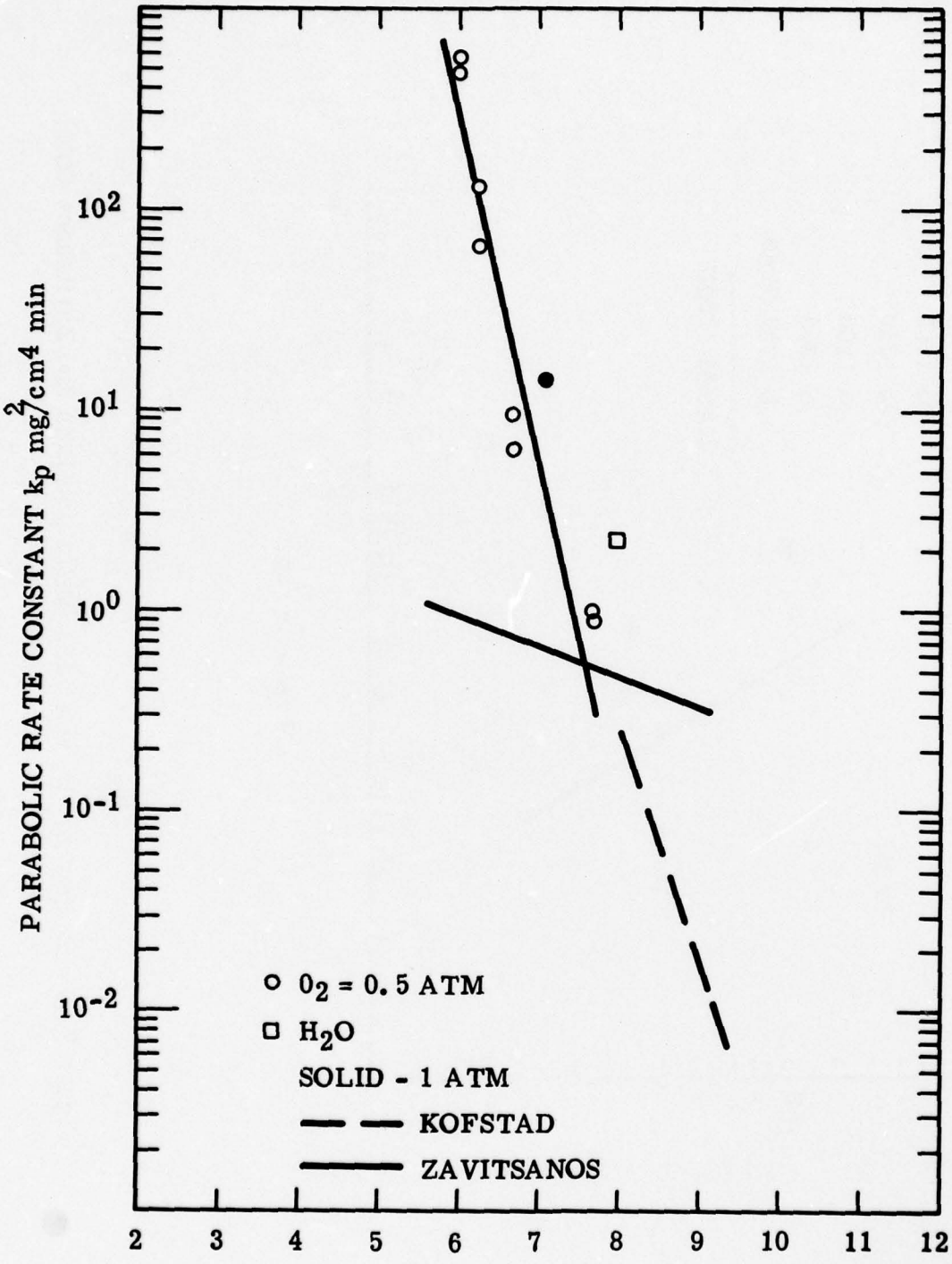

Figure 2-4. Comparison Between SAI, Kofstad and Zanitsanos Rate Data

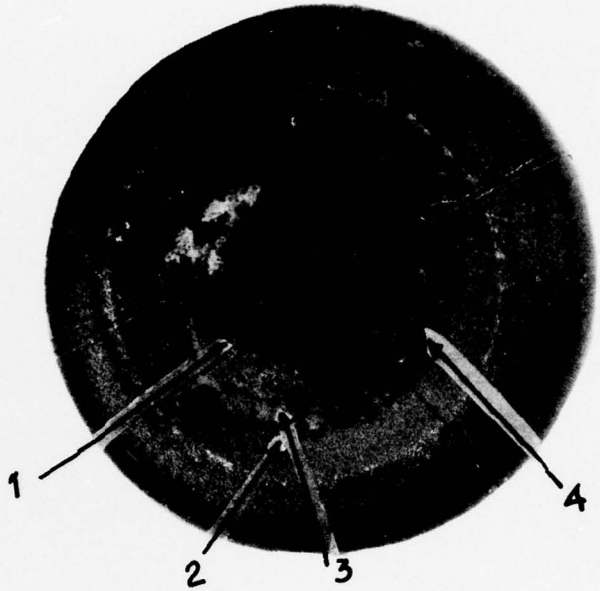

FIGURE 2-5 VIEW OF TEST SAMPLE 28A, AEDC TEST (2/26/72) SHOWING IGNITION AND DUST ROUGHENED SURFACE

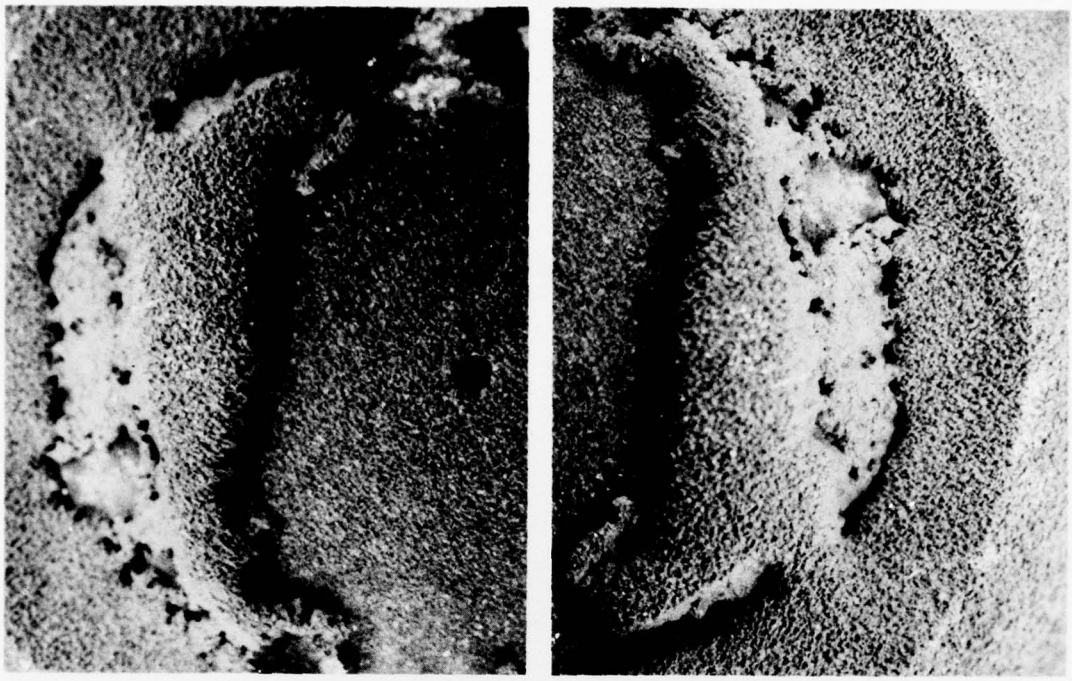

1 3

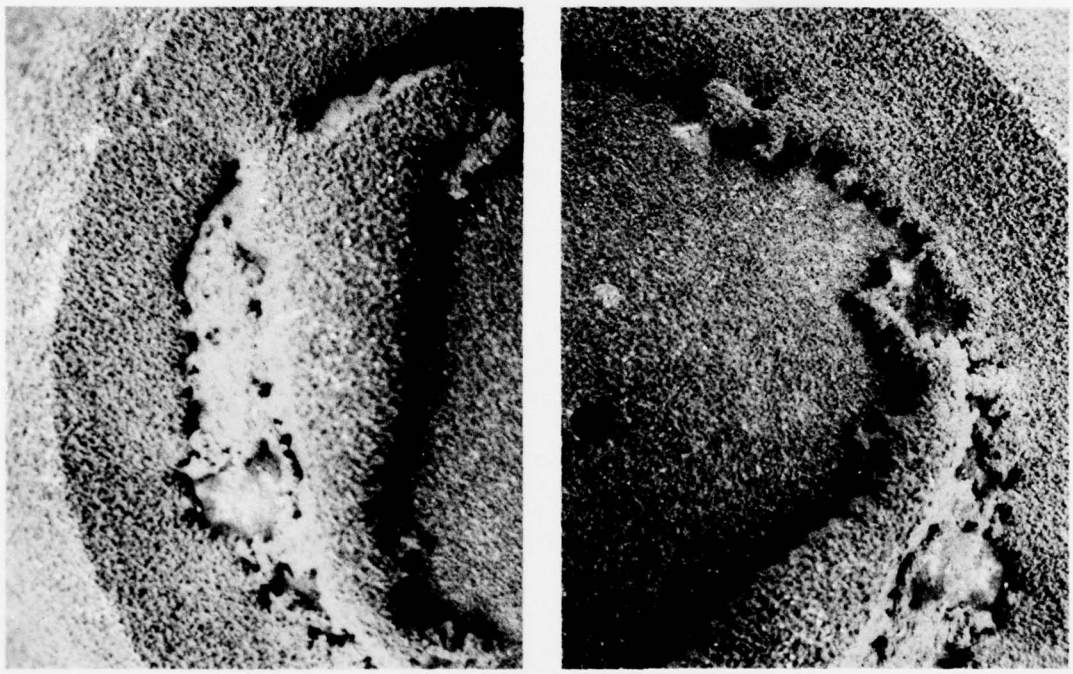

2 4

FIGURE 2-6 DETAILED VIEWS OF SURFACE ROUGHNESS

3.0 EVALUATION OF OXIDATION INFLUENCE ON MATERIAL THICKNESS REQUIREMENTS

3.1 Introduction

The stagnation point and cone sidewall response is calculated for a typical configuration and trajectory to assess the influence of oxidation response on the temperature history of the material. As noted earlier the stagnation point is examined for ignition probability and the sidewall for strength reduction.

The configuration chosen is shown schematically in Figure 3-1. The nose radius is 5.9 inches and the cone angle is 11^{o}. These are typical configurations. A typical velocity altitude profile is shown in Figure 3-2.

3.2 Stagnation Point Temperature Response

The stagnation point heat transfer used to produce Temperature-Altitude curves (Figure 3-3) is the additive sum of the aerodynamic heat transfer and the conversion of particle energy to heating rate under normal impact conditions, less reradiated energy, i.e.

$$\dot{q}_n = \dot{q}/_{\Delta h} \ (h_r - h_w) + \dot{q}_{KE} - \dot{q}_{rr}$$

and

$$\dot{q}_{KE} = \frac{\rho cl \ V^3 \sin\theta}{2gJ} \ x \ f(\theta)$$

where $f(\theta)$ is taken from a correlation of MM III dust tests at the Boeing Co. and the Arnold Engineering Test Center. At 90^{o} the value of $f(\theta)$ is 0.7, which implies that 70% of the dust kinetic energy is converted to thermal energy and is treated as a net heat transfer rate. The reradiation heat transfer is treated in the standard fashion with emmittance of 0.3. This is probably low for the roughened or oxidized surface of the material.

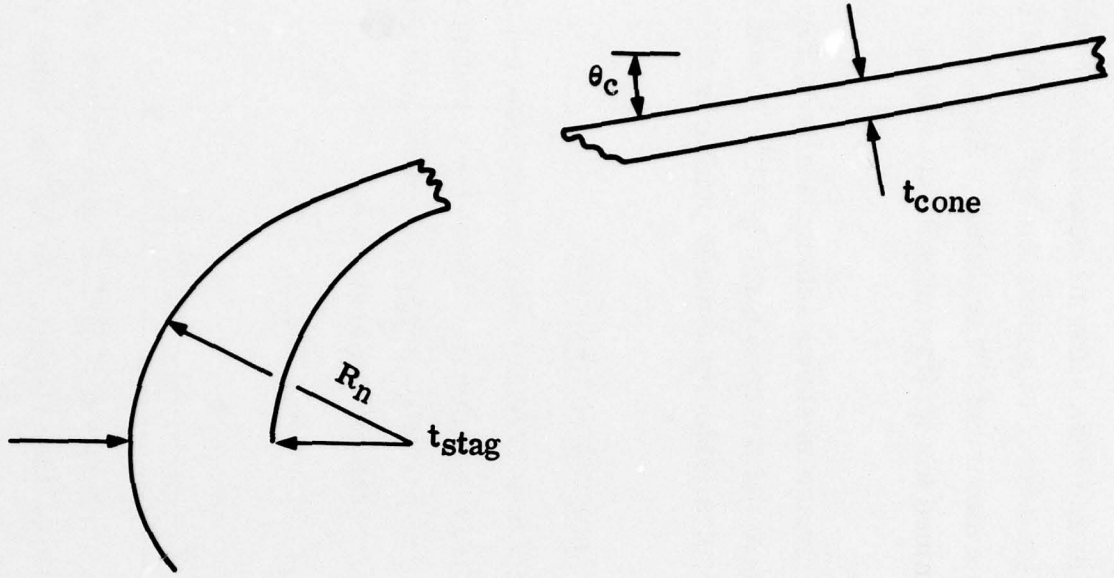

Figure 3-1. Schematic of Typical Vehicle

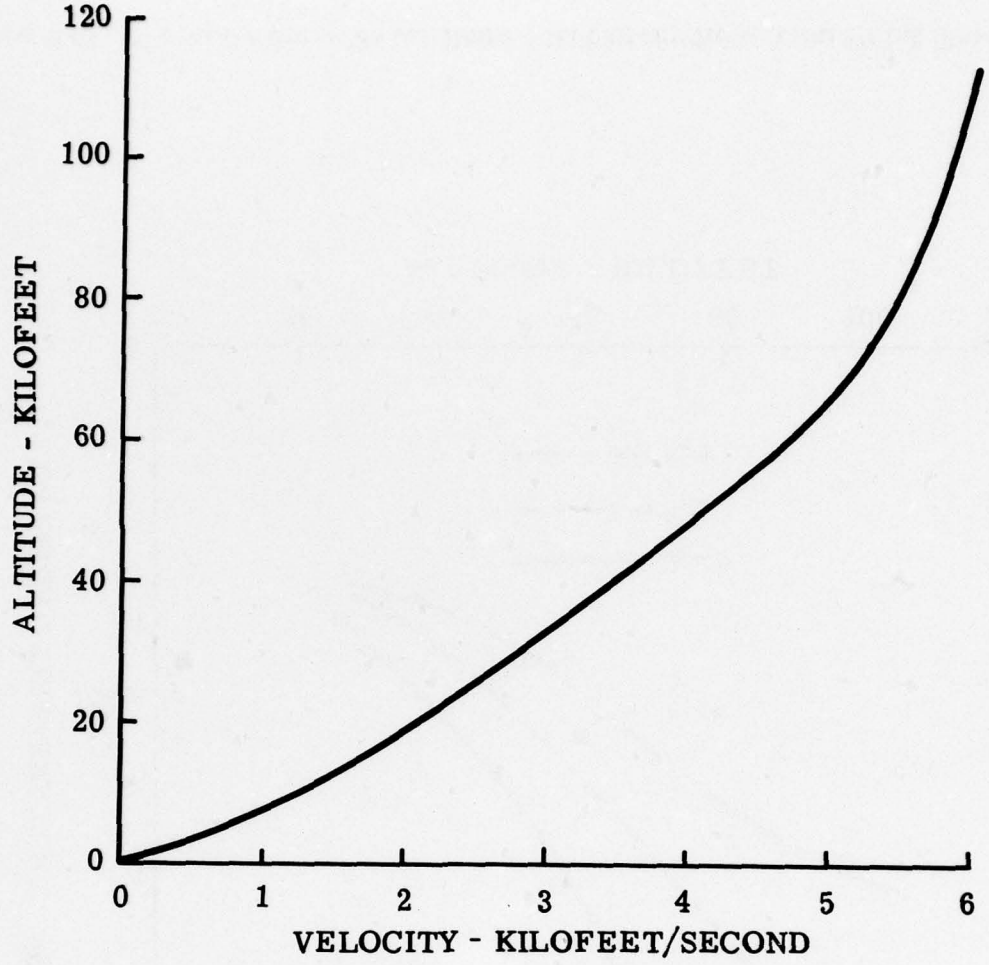

Figure 3-2. Velocity Vs Altitude for a Typical Boost, Phase Vehicle

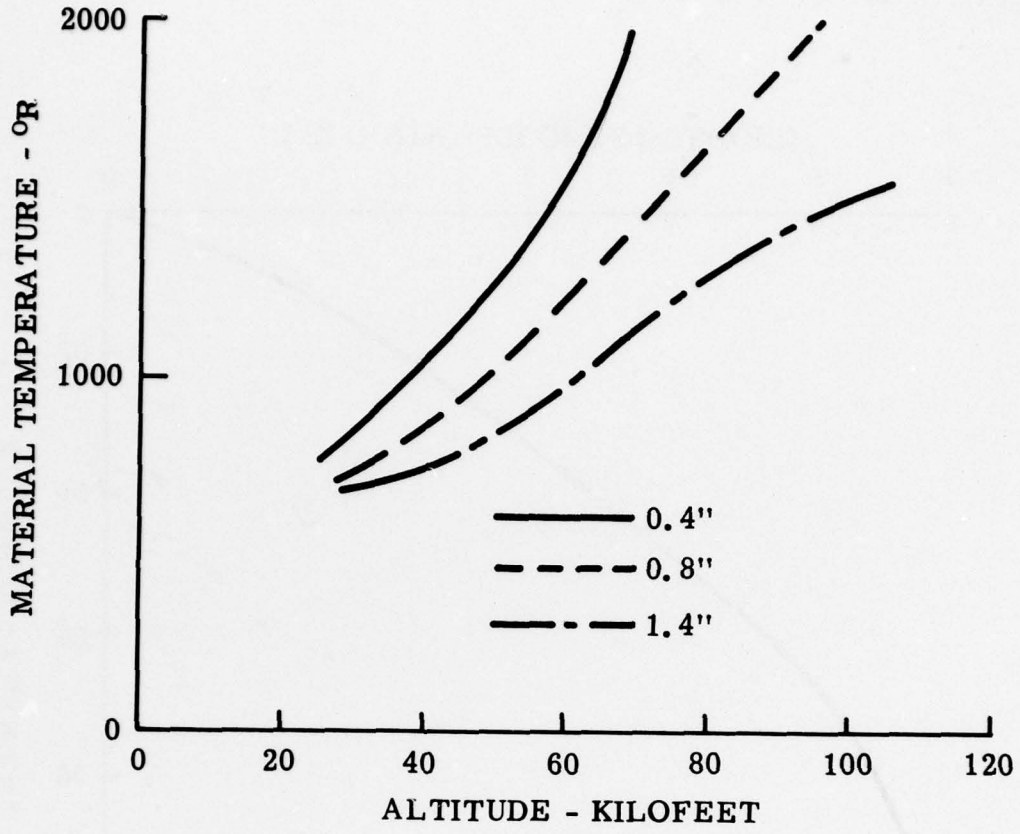

Figure 3-3. Temperature Vs Altitude for Three Stagnation Point Thicknesses

For the trajectory conditions flown and for the dust particle density used the peak heat transfer rate is 126 Btu/ft^2 sec, with 73 Btu/ft^2 sec from dust particle impact and 53 Btu/ft^2 sec from aerodynamic heating. Invoking the condition that $T_{max} < 2460$ R. to prevent titanium ignition results in a thickness requirement of 1.4 at the stagnation point, without consideration given to an increased heating due to oxidation of the titanium.

As shown in (2), the additional heat transfer due to oxidation at temperatures below 2000 F are negligible.

For this application sufficient material thickness to maintain $T_s < 2000$ F results in very low ignition probability.

3.3 Conical Section

The analysis of the conical section is shown in Figure 3-4. Surface temperature predictions for three thickness-distributions at the maximum heat transfer point on the cone show temperatures well below ignition, and well below conditions where oxidation heat transfer rates result in strength reductions. The thickness requirements for structural adequacy of the design are limiting conditions for the cone, and oxidation heat transfer rates do not establish a new thickness requirement.

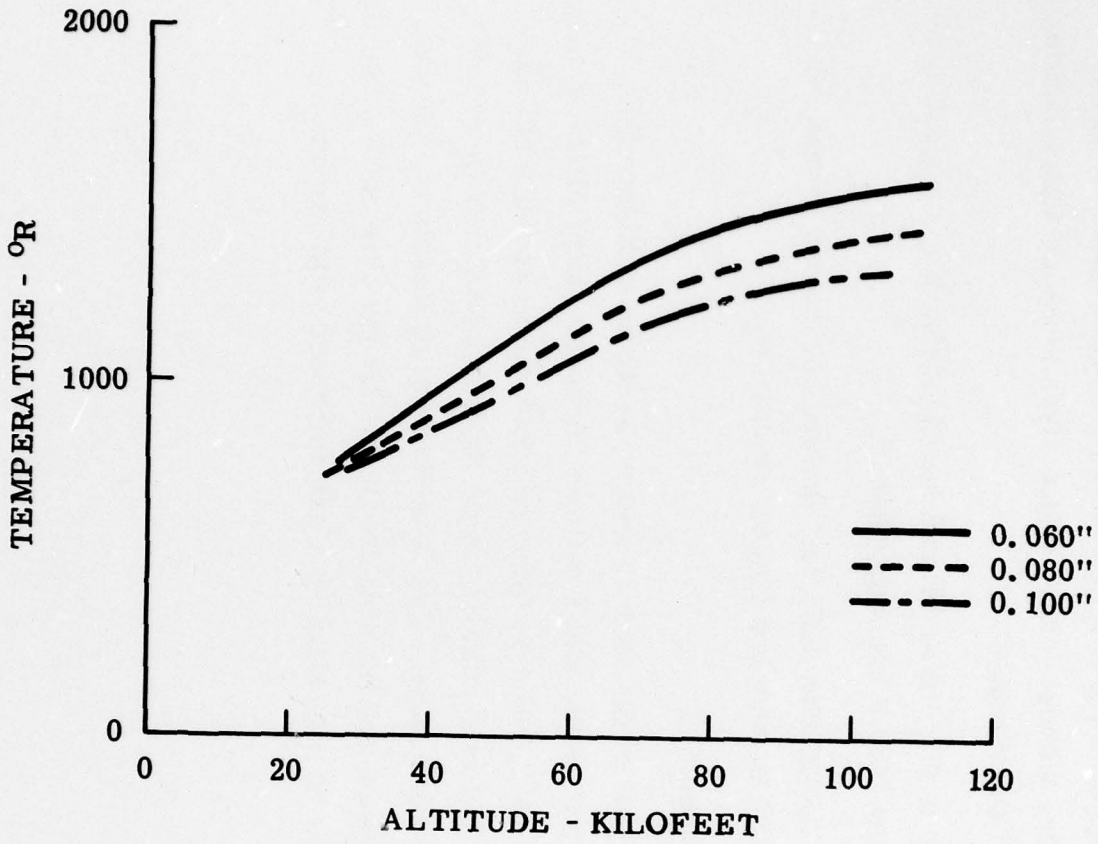

Figure 3-4. Temperature Response of Cone Tangency for 3 Thicknesses

4.0 CONCLUSIONS:

The very brief study was directed at a determination of ignition probability for titanium in a sphere cone configuration passing through a dust, water and ice laden environment.

We used previous test data on titanium oxidation rates and new test data obtained by SAI/Santa Ana to evaluate heat release due to oxidation, and combined this with the normal convective heating and fractional conversion of dust water and ice kinetic energy to heat evaluate the temperature response of a stagnation region and a conical wall region with varying thickness.

From these evaluations we can draw the following conclusions:

1. Titanium oxidation, assuming a fresh titanium surface and scale forming rate constant, will not increase heat transfer rates and cause ignition.

2. The heat transfer rates at the stagnation point of the configuration are dominated by the conversion of particulate energy.

Further studies which would be fruitful in permitting reduced stagnation point thicknesses are in the area of particulate energy conversion to heating rate. This will be especially true for more severe dust environments.

REFERENCE LIST

1. R. J. Sullivan, "Heating Augmentation Study", GE-RESD Document 72SD2166A, 28 September 1973.

2. Dunbar, et. al., "Titanium Response to Simulated Nuclear Cloud Particle Environment", SAI 78-561-LA, 31 August 1977.

3. J. Stringer, J. Acta Metallurgica, 8, 758 (1960).

4. Rosa, C. J., Personal visit and communication.

5. P. Zavitsanos / GE-RESD personal communication.

NOMENCLATURE:

SYMBOL	IDENTIFICATION	UNITS
g	Gravitational constant	ft/sec^2
h	Enthalpy	Btu/lb
k	Rate constant	$g^2\ cm^{-4}\ sec^{-1}$
P	Pressure	Atmospheres microns (10^{-6} meters of Hg.)
$\dot{q}$	Heat transfer rate	Btu/ft^2 sec
V	Velocity	ft/sec
R	Universal gas constant	cal/mole K
T	Temperature	degrees K or R
t	Time of exposure to oxidation	seconds/minutes
W	Weight gain due to oxide formation	grams

SUBSCRIPTS

m	Oxygen dissolution rate constant
n	Net heating rate
p	Parabolic value of rate constant
r	recovery
s	Scale forming rate constant
w	Wall
rr	re-radiation heat transfer
KE	fraction of kinetic energy converted to heat

DISTRIBUTION LIST

DEPARTMENT OF DEFENSE

Assistant to the Secretary of Defense
Atomic Energy
ATTN: Executive Assistant

Defense Advanced Rsch. Proj. Agency
ATTN: TIO

Defense Communications Agency
ATTN: CCTC

Defense Documenation Center
12 cy ATTN: DD

Defense Intelligence Agency
ATTN: DB-4D
ATTN: DT-2
ATTN: DT-1C

Defense Nuclear Agency
ATTN: STSP
ATTN: SPAS
ATTN: SPTD
ATTN: SPSS
ATTN: DDST
4 cy ATTN: TITL

Field Command
Defense Nuclear Agency
ATTN: FCPR

Joint Strategic Tgt. Planning Staff
ATTN: JLTW-2
ATTN: JPTM

Livermore Division, Field Command, DNA
ATTN: FCPRL

Under Secretary of Defense for Rsch. & Engrg.
ATTN: Engineering Technology, J. Persh
ATTN: Strategic & Space Systems (OS)

DEPARTMENT OF THE ARMY

BMD Advanced Technology Center
Huntsville Office
Department of the Army
ATTN: ATC-T, M. Capps

BMD Systems Command
Department of the Army
ATTN: BMDSC-H, N. Hurst

Deputy Chief of Staff for Rsch. Dev. & Acq.
Department of the Army
ATTN: Nuclear Team

Harry Diamond Laboratories
Department of the Army
ATTN: DELHD-N-TF
ATTN: DELHD-N-P, J. Gwaltney

DEPARTMENT OF THE ARMY (Continued)

U.S. Army Ballistic Research Labs
ATTN: DRDAR-BLV, W. Schuman, Jr.
ATTN: DRDAR-BLE, J. Keefer
ATTN: DRDAR-BL, R. Eichelberger
ATTN: DRDAR-BLV
ATTN: DRDAR-BLT, R. Vitali
ATTN: DRXBR-TB, J. Frasier

U.S. Army Material & Mechanics Rsch. Ctr.
ATTN: DRXMR-HH, J. Dignam

U.S. Army Materiel Dev. & Readiness Cmd
ATTN: DRCDE-D, L. Flynn

U.S Army Missile R&D Command
ATTN: DRDMI-XS
ATTN: DRDMI-TKP, W. Thomas
ATTN: DRDMI-TRR, B. Gibson

DEPARTMENT OF THE NAVY

Naval Research Laboratory
ATTN: Code 6770, G. Cooperstein
ATTN: Code 2627
ATTN: Code 7908, A. Williams

Naval Surface Weapons Center
ATTN: Code K06, C. Lyons
ATTN: Code F31
ATTN: Code R15, J. Petes

Office of Naval Research
ATTN: Code 465

Office of the Chief of Naval Operations
ATTN: R. Blaise
ATTN: OP 604
ATTN: OP 604C3, R. Piacesi

Strategic Systems Project Office
Department of the Navy
ATTN: NSP-272

DEPARTMENT OF THE AIR FORCE

Aeronautical Systems Division, AFSC
2 cy ATTN: ENFTV, D. Ward

Air Force Flight Dynamics Laboratory, AFSC
ATTN: FXG
ATTN: J. Wood
ATTN: S. Inouye

Air Force Materials Laboratory, AFSC
ATTN: MRC, D. Schmidt
ATTN: MBE, G. Schmitt
ATTN: T. Nicholas

Air Force Systems Command
ATTN: SOSS
ATTN: XRTO

DEPARTMENT OF THE AIR FORCE (Continued)

Air Force Weapons Laboratory, AFSC
ATTN: DYV, A. Sharp
ATTN: DYT
ATTN: DYV
ATTN: SUL
ATTN: DYS
ATTN: Technical Review
ATTN: Dr. Minge
2 cy ATTN: NTO

Arnold Engineering Development Center, AFSC
Department of the Air Force
ATTN: XRRP

Deputy Chief of Staff
Research, Development, & Acq.
Department of the Air Force
ATTN: AFRDQSM
ATTN: AFRD
ATTN: AFRDPX
ATTN: AFRDQ

Deputy Chief of Staff
Operations, Plans and Readiness
Department of the Air Force
ATTN: AFXOOSS

Foreign Technology Division, AFSC
ATTN: SDBG
ATTN: TQTD
ATTN: SDBS, J. Pumphrey

Space & Missile Systems Organization
Air Force Systems Command
ATTN: DYS

Space & Missile Systems Organization
Air Force Systems Command
ATTN: MNNH
ATTN: MNNR

Strategic Air Command
Department of the Air Force
ATTN: DOXT
ATTN: XPQM
ATTN: XOBM
ATTN: XPFS

DEPARTMENT OF ENERGY

Department of Energy
ATTN: Office of Military Application

DEPARTMENT OF DEFENSE CONTRACTORS

Acurex Corporation
ATTN: C. Nardo
ATTN: J. Huntington
ATTN: R. Rindal
ATTN: J. Cortney

Aerospace Corporation
ATTN: J. McClelland
ATTN: H. Blaes
ATTN: R. Strickler
ATTN: R. Crolius
ATTN: W. Mann
ATTN: R. Mortensen
ATTN: W. Barry

DEPARTMENT OF DEFENSE CONTRACTORS (Continued)

Avco Research & Systems Group
ATTN: J. Stevens
ATTN: Document Control
ATTN: W. Broding
ATTN: J. Gilmore

Boeing Company
ATTN: R. Dyrdahl
ATTN: E. York
ATTN: B. Lempriere
ATTN: R. Homes

California Research & Technology, Inc.
ATTN: K. Kreyenhagen

University of Dayton
Industrial Security Super., KL-505
ATTN: D. Gerdiman
ATTN: H. Swift

Effects Technology, Inc.
ATTN: R. Parisse
ATTN: R. Wengler

General Electric Co.
Space Division
ATTN: D. Edelman
ATTN: C. Anderson
ATTN: G. Harrison

General Electric Co.
Re-Entry & Environmental Systems Div.
ATTN: P. Cline
ATTN: R. Sullivan

General Electric Co.-TEMPO
Center for Advanced Studies
ATTN: DASIAC

Kaman Sciences Corporation
ATTN: D. Sachs
ATTN: J. Hoffman
ATTN: T. Meagher
ATTN: J. Keith
ATTN: F. Shelton

Lawrence Livermore Laboratory
University of California
ATTN: L-92, C. Taylor
ATTN: G. Staihle
ATTN: L-125, J. Keller
ATTN: L-216, J. Knox

Lockheed Missiles & Space Co., Inc.
ATTN: R. Walz

Lockheed Missiles and Space Co., Inc.
ATTN: F. Borgardt

Lockheed Missiles and Space Co., Inc.
ATTN: T. Fortune

McDonnell Douglas Corporation
ATTN: L. Cohen
ATTN: D. Hender
ATTN: D. Giedt
ATTN: G. Johnson

DEPARTMENT OF DEFENSE CONTRACTORS (Continued)

National Academy of Sciences
National Materials Advisory Board
ATTN: D. Groves

Physics International Company
ATTN: J. Shea

Prototype Development Associates, Inc.
ATTN: J. McDonald

R & D Associates
ATTN: W. Graham, Jr.
ATTN: F. Field

Sandia Laboratories
Livermore Laboratory
ATTN: Library & Security Classification Div.
ATTN: H. Norris, Jr.

Science Applications, Inc.
ATTN: G. Burghart
ATTN: C. Swain

Southern Research Institute
ATTN: C. Pears

DEPARTMENT OF DEFENSE CONTRACTORS (Continued)

SRI International
ATTN: D. Curran
ATTN: P. Dolan
ATTN: G. Abrahamson
ATTN: H. Lindberg

Systems, Science & Software, Inc.
ATTN: G. Gurtman
ATTN: R. Duff

TRW Defense & Space Sys. Group
ATTN: G. Arenguren
ATTN: A. Zimmerman
ATTN: M. Siezew
ATTN: M. King

TRW Defense & Space Sys. Group
San Bernardino Operations
ATTN: W. Polich
ATTN: L. Berger
ATTN: E. Allen
ATTN: V. Blankenship
ATTN: E. Wong